

DETECTION OF ABSORPTION FEATURES IN THE X-RAY SPECTRUM OF THE NARROW-LINE QUASAR PG 1404+226: POSSIBLE EVIDENCE FOR ACCRETION DISK WINDS

SURAJIT DASGUPTA ¹, A. R. RAO ¹, G. C. DEWANGAN ², V. K. AGRAWAL ³

ABSTRACT

We present the results of an analysis of data from *XMM-Newton* and *CHANDRA* observations of the high luminosity narrow-line quasar PG 1404+226. We confirm a strong soft X-ray excess in the X-ray spectrum and we find rapid variability (a factor of two in about 5000 s). When the X-ray spectrum is fit with a two component model which includes a power-law and a blackbody component, we find that low energy absorption lines are required to fit the data. If we interpret these lines as due to highly ionized species of heavy elements in an outflowing accretion disk wind, an outflow velocity of ~ 26000 km s⁻¹ could be derived. One interesting feature of the present observation is the possible detection of variability in the absorption features: the absorption lines are visible only when the source is bright. From the upper limits of the equivalent widths (EW) of the absorption lines during the low flux states and also from the model independent pulse height ratios, we argue that the strength of absorption is lower during the low flux states. This constraints the physical size of the absorbing medium within 100 Schwarzschild radius (R_g) of the putative supermassive black hole. We also find a marginal evidence for a correlation between the strength of the absorption line and the X-ray luminosity.

Subject headings: galaxies: active — quasars: individual(PG 1404+226) — X-rays: galaxies

1. INTRODUCTION

Narrow-line Seyfert 1 galaxies (NLS1s) have very remarkable X-ray properties: they show evidence for strong excess of soft X-rays (dominant below ~ 2 keV) above the hard X-ray continuum extrapolation and rapid X-ray variability (Boller et al. 1996). Complex absorption features are also common in many of these sources. Recently Pounds et al. (2003a,b) detected several absorption lines in the narrow emission line quasars PG 1211+143 and PG 0844+349 which are blue-shifted indicating relativistic outflow of highly ionized material. They suggest that these outflows form a significant component in the mass and energy budgets of systems accreting at or above the Eddington rate (King & Pounds 2003).

PG 1404+226 ($V=15$, $M=-23.4$, $z=0.098$) is one of the most extreme narrow line Fe II quasar. Its $H\beta$ FWHM is 880 km s⁻¹ (Boroson & Green 1992). The *ROSAT* spectrum (0.1 - 2 keV) of PG 1404+226 is steep ($\Gamma \sim 3$) and shows rapid (factor of 2 in 10 hours) flux variability. Moreover flux selected spectral analysis revealed the presence of an absorption edge around 0.8 - 1 keV whose energy shift to higher value when the source brightens (Ulrich & Molendi 1996). The X-ray spectrum of PG 1404+226 was variable during an *ASCA* observation (Comastri et al. 1997; Ulrich et al. 1999, hereafter U99) and characterized by a strong soft excess below 2 keV whose luminosity in 0.4 - 2 keV band (7×10^{43} ergs s⁻¹) was a factor of 3 greater than 2 - 10 keV luminosity. Comastri et al. (1997) have also found an absorption edge at 1.07 keV and they suggested an over abundance of iron. Leighly et al. (1997) compared the absorption

feature found in *ASCA* spectrum with absorption by ionized oxygen and derived a high velocity of ionized outflow from that object.

In this *Letter* we present the *XMM-Newton* and *CHANDRA* observations of PG 1404+226. We detect absorption features in the *XMM-Newton* data and find some evidence for such lines in the *CHANDRA* data. We have reanalyzed *ASCA* data which corroborates this conclusion. The source shows high variability in all the three observations and most remarkably, the line features show variability in time scales of ~ 5000 s, giving a direct dynamical size constraint of $100 R_g$ for the absorbing medium.

2. DATA AND ANALYSIS

PG 1404+226 was observed by *XMM-Newton* on 2001 June 18 using the European Photon Imaging Camera (EPIC), and the reflection grating spectrometer (RGS) for about 21 ks. RGS data are not useful because of poor signal to noise ratio. The observation data files were processed and filtered using the same criterion as discussed in Dasgupta et al. (2004). The high energy particle background flaring intervals were excluded. This resulted in 'good' exposure time of ~ 14 ks for the EPIC-PN. The net count rate is 0.66 s⁻¹. The Chandra High Energy Transmission Grating Spectrometer (HETGS) observation of this source was performed during 2000 July 22 for a total duration of 80 ks. The spectrum is created using 0th order image of the source because of low counts collected in HEG and MEG. PG 1404+226 was observed by *ASCA-GIS/SIS* on 1994 July 13-14. In this paper SIS data are reanalyzed. The SIS was operating in 1-CCD mode and the data were collected in Faint mode. Standard criterion for good time selections (U99) have been applied.

EPIC-PN light curves of bin size 500 s (background subtracted) of PG 1404+226 in the energy range 0.3 - 1 keV (soft), 1 - 10 keV (hard) are plotted in Figure 1. The energy bands were chosen to separate approx-

¹ Department of Astronomy and Astrophysics, Tata Institute of Fundamental Research, Mumbai-400005, India, surajit@tifr.res.in, arrao@tifr.res.in

² Department of Physics, Carnegie Mellon University, Pittsburgh, PA 15213 USA, gulabd@cmu.edu

³ Inter-University Center for Astronomy and Astrophysics, Pune-411007, India, agrawal@iucaa.ernet.in

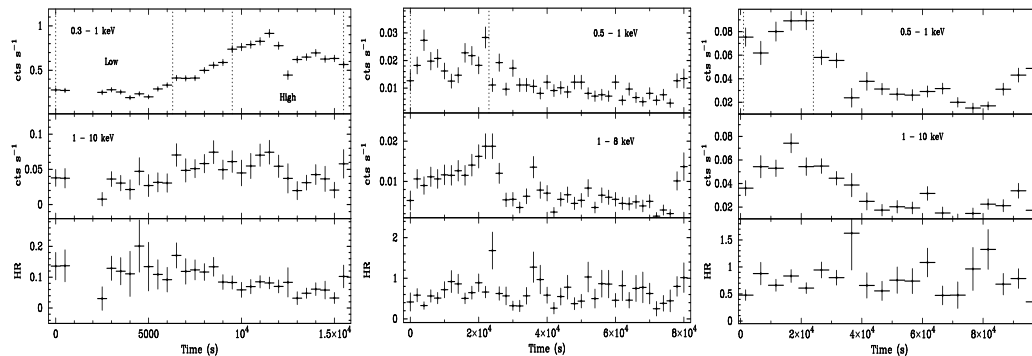


FIG. 1.— (a) EPIC-PN 500s bin (left), (b) CHANDRA-ACIS 2000s bin (middle), and (c) ASCA-SIS (SIS0 AND SIS1 added) 5000s bin light curves and the corresponding hardness ratio (see text).

imately the two spectral components – a power-law and a soft excess component generally observed from NLS1s (Leighly 1999). It is evident that the X-ray emission from PG 1404+226 varied strongly during the *XMM-Newton* observation. The average count rates in the low and high flux states (demarcated by dotted lines in Figure 1) are 0.26 ± 0.01 and 0.69 ± 0.02 s^{-1} respectively in soft band, 0.029 ± 0.007 and 0.042 ± 0.007 s^{-1} respectively in hard. The hardness ratio (defined as the ratio between flux of hard band to that of soft band) is decreasing with time, implying that the spectrum softens in the high state. *ACIS* and *SIS* light-curves (Figure 1) show similar timescale of variability.

Photon energy spectra of PG 1404+226 and associated background spectra were accumulated from the EPIC-PN, ASCA-SIS and CHANDRA-ACIS data. The pulse invariant channels were grouped such that each bin contains at least 20 counts. Data above 8 keV are not used in spectral analysis because background counts are comparable with source counts in this regime. All the spectral fits were performed with the XSPEC 11.2.0 and using the χ^2 statistics. The quoted errors on the best-fit model parameters are at the 90% confidence level ($\Delta\chi^2 = 2.7$). Luminosities are derived assuming isotropic emission. A value for the Hubble constant of $H_0 = 50$ km s^{-1} Mpc^{-1} and a standard cosmology with $q_0 = 0$ has been adopted.

We fitted a redshifted powerlaw model with a Galactic N_H of 2×10^{20} cm^{-2} (Elvis et al. 1989) to the EPIC-PN spectrum in the energy range of 2 - 8 keV. This provides an acceptable fit ($\chi^2/dof \simeq 26/24$ and $\Gamma \sim 1.72$). There is a excess emission above 6.5 keV, but addition of a narrow redshifted Gaussian line near 6.4 keV does not improve the fit ($\Delta\chi^2_p < 4$). Extrapolation of the best fitting 2 - 8 keV power law to 0.3 keV shows a huge soft excess in the spectrum. Adding a redshifted blackbody gives a reasonable fit ($\chi^2/dof \sim 189/162$, $\Gamma \sim 1.46$, $kT_{bb} \sim 108$ eV). The model (model a in Figure 3) leaves significant residuals in the 0.8 - 1.2 keV (observed frame) band and at 3 keV. Addition of Gaussian absorption lines at 1, 1.2, and 3 keV to the previous model (hereafter model e) gives a good fit with $\chi^2(dof) \sim 134(156)$ (Figure 2). All the derived parameter values along with the errors are given in the Table 1. We have fitted several other models to the data based on the previous results reported on the same source (Figure 3). An absorption component (model *absori* in XSPEC) along with the blackbody and power-law does improve the fit ($\chi^2/dof \sim 174/158$ dof) but the

absorption feature still remains (model b). Over abundance of iron (U99) cannot handle the absorption feature completely ($\chi^2/dof \sim 154/159$, the iron abundance became more than 25 times solar abundance). Adding an edge with the absorption model (with super iron abundance) does not improve the fit ($\Delta\chi^2 \sim 2$). Adding an edge at ~ 1 keV with the two component model (model c) can handle the absorption feature at 1 keV ($\chi^2/dof \sim 153/160$) but the 1.2 keV feature still remains. But adding another edge (model d) for the ~ 1.2 keV feature worsen the fit ($\Delta\chi^2 \sim 1$). One edge and one line also cannot handle the situation. But when we adopt the model with two absorption lines the fit is improved drastically ($\chi^2/dof \sim 144/158$) and the residuals around 1 keV vanished. Adding another absorption line at ~ 3 keV improves the fit further ($\Delta\chi^2 \sim 10$).

To investigate whether the flux variability is due to changes in the spectral parameters we have carried out spectral analysis at low and high flux levels. We extracted two average spectra covering 0 - 6.5 ks (high flux state) and 9.5 - 15.5 ks (low flux state) in the 0.3 - 8 keV band. The average EPIC-PN count rates are 0.26 ± 0.01 s^{-1} (low flux state) and 0.69 ± 0.02 s^{-1} (high flux state). We fit the data using model e. The fit parameters and the observed fluxes in the two flux states are given in Table 1. The observed flux in the 0.3 - 8.0 keV range varied by a factor of 2.6 during the high and low flux states. The blackbody flux varied by a factor of 3 whereas the power-law flux varied by a factor of 1.7. The spectral

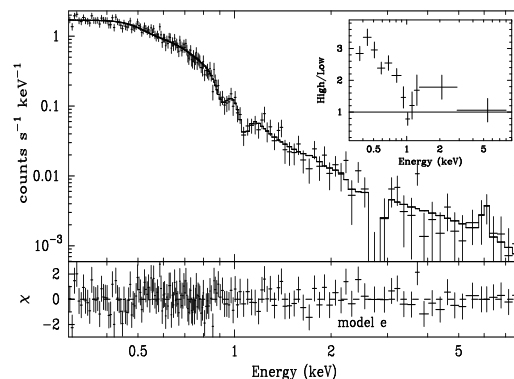


FIG. 2.— 0.3 - 8 keV EPIC-PN spectrum and best fitted model (model e, see text) and the residual spectrum (lower panel). The panel inside is the PHA ratio of high and low flux states.

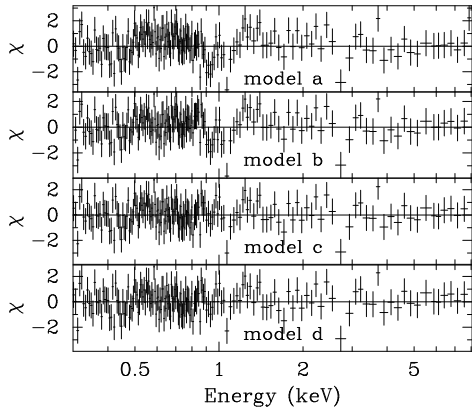


FIG. 3.— 0.3 – 8 keV EPIC-PN residual spectra fitted with different models (see text).

parameters are consistent with each other at 90% confidence level. Since the spectral parameters and the normalizations are strongly coupled to each other, we can only conclude that the soft and hard components varied at different ratios. The absorption lines, on the other hand, are not required at the low flux level. We have included two lines (0.99, 1.17 keV) to get an estimate of the upper limits to the fluxes. The 90% confidence upper limits on the line fluxes during the low flux state are distinctly lower than those found for the high flux state. The upper limit on the EW has an overlap with the 90% confidence error for that in the high flux level. To understand the spectral variability in more detail, we plot the PHA ratio of high and low flux states with energy (Figure 2, inner panel). While the flux difference in the soft emission is remarkable, the variability above 1 keV is much lower. There is a clear dip at around 1 keV indicating that absorption is significantly high in the high flux state.

To corroborate these findings we have analysed the spectra from the *CHANDRA* and *ASCA* data. The detection significance above 1 keV in these two data sets is poor and we find a marginal evidence for the absorption lines in the time-averaged data. Results of the spectral fits to the high flux states in these two data sets (marked in Figure 1) are presented in Table 1. The absorption lines are detected in the *ASCA* data ($\Delta\chi^2 \sim 10$) and there is a marginal evidence for these lines in the *CHANDRA* data. The line energies and identifications in case of *ASCA* data are different from that by Leighly et al. (1997) probably because of different continuum modeling. It is clear from Table 1 that the strength of the absorption lines increased when the flux increased. It is interesting to investigate whether these changes are correlated with each other. For this purpose we have divided the whole region into several parts of 1000 s duration. The energy channels were appropriately grouped to achieve a good signal-to-noise (a minimum of 5 counts per energy channel). All the spectra are fitted with the same model mentioned above (with C-statistics). All the parameters except the normalizations of blackbody, power-law and absorption lines are fixed to the values found from the fit result of the average spectrum. The relative normalization between the absorption lines are kept fixed. The variation of the free parameters with

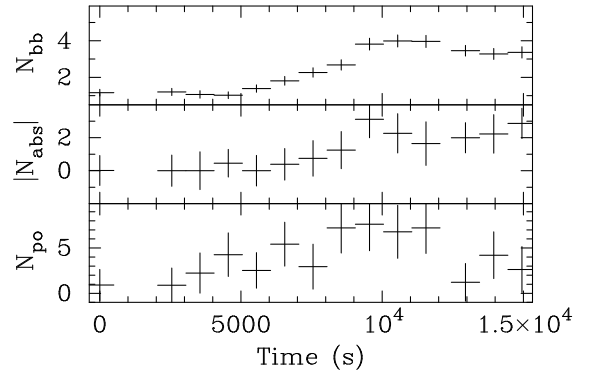


FIG. 4.— Variability of normalizations (units defined in the footnote of Table 1) of power-law (N_{po}), blackbody (N_{bb}) and absorption line at 1 keV (N_{abs}) with time.

time is shown in Figure 4. It is clear that all the free parameters vary with time in a same fashion and the variations are similar to the count-rate variations. The black body flux is correlated with the line flux with a rank correlation coefficient of 0.79 (probability 8×10^{-4}).

3. DISCUSSION

The spectroscopic analysis carried in this paper using *XMM-Newton* data revealed three absorption line features at $\sim 1.0, 1.17, 3$ keV with EW of 45, 60, and 364 eV, respectively. The line energy and EW are comparable to that found in PG 1211+143 by (Pounds et al. 2003a). We have made similar identifications for the spectral lines detected in PG 1404+226 and they are given in Table 2. For some of the lines a few possible alternate line identifications are also given. For the two strongest lines detected by the EPIC-PN (0.99, 1.17 keV) we derive outflow velocities of 25700^{+3300}_{-6500} and 43500^{+5900}_{-5900} km s $^{-1}$. However if we consider the 1.17 keV is originated from the line Ne IX 1s-3p (1.073 keV) then the measured outflow velocity will be 27000^{+5500}_{-5500} km s $^{-1}$. Though there is an indication of different velocities from the other line identifications, we cannot rule out the possibility of all lines originating from similar velocity structures due to the much lower significance level of detection of these lines.

The more striking result of our analysis is the possible detection of line variability. From the model independent PHA ratio, we can see that there is strong spectral variability and the absorption line strength (EW) are also different in the two spectral states. The time scale of variation (~ 5000 s) suggest that the absorption features originate in the warm absorbing material located within $\sim 100 R_g$ from the central source (for an estimated black hole mass of $5.2 \times 10^6 M_\odot$). Since it is unlikely that the physical condition of the absorbing material can change with the increase in the luminosity, we postulate that high luminosity drives stronger winds either due to radiation pressure or as a result of magnetic reconnection. The insufficient spectral resolution of the instrument leads to large uncertainty of the line energy. Uncertainty in the central energy, shape, and possible multiple absorption components in a single feature may lead to incorrect velocities or identifications. But in spite of these limitations, rapid variability of line strength is seen.

TABLE 1
BEST-FIT SPECTRAL PARAMETERS OF PG 1404+226.

Component	Parameter	EPIC-PN ^a		ASCA-SIS ^a	CHANDRA-ACIS ^a
		Average	High	Low	High
Blackbody	kT (eV)	114^{+2}_{-2}	112^{+2}_{-2}	119^{+5}_{-5}	120^{+20}_{-20}
	n_{bb} ^b	$2.97^{+0.09}_{-0.09}$	$4.34^{+0.17}_{-0.17}$	$1.33^{+0.90}_{-1.00}$	$7.46^{+4.18}_{-2.60}$
Power law	f_{bb} (0.3-8 keV) ^e	10.33	14.82	4.86	25.82
	Γ	$1.59^{+0.13}_{-0.12}$	$1.62^{+0.46}_{-0.16}$	$1.27^{+0.27}_{-0.20}$	$1.95^{+0.43}_{-0.42}$
	n_{pl} ^c	$4.42^{+1.25}_{-0.94}$	$5.05^{+2.30}_{-1.70}$	$1.97^{+1.60}_{-0.90}$	$37.1^{+19.1}_{-14.5}$
	f_{pl} (0.3-8 keV) ^e	2.48	2.75	1.55	15.32
Gaussian 1	E_{line} (keV)	$3.07^{+0.06}_{-0.16}$	$3.03^{+0.10}_{-0.32}$	---	---
	n_g ^d	$-2.80^{+1.56}_{-1.52}$	$-4.00^{+2.98}_{-3.61}$	---	---
Gaussian 2	EW (eV)	-348^{+194}_{-189}	-438^{+328}_{-395}	---	---
	E_{line} (keV)	$1.17^{+0.02}_{-0.02}$	$1.17^{+0.03}_{-0.02}$	1.17	$1.59^{+0.10}_{-0.08}$
	n_g ^d	$-6.67^{+2.13}_{-2.03}$	$-12.43^{+3.54}_{-3.76}$	> -4.80	$-15.7^{+12.3}_{-22.2}$
Gaussian 3	EW (eV)	-60^{+19}_{-18}	-84^{+24}_{-25}	-22^{+22}_{-47}	-87^{+87}_{-68}
	E_{line} (keV)	$1.00^{+0.01}_{-0.02}$	$1.00^{+0.01}_{-0.02}$	0.99	$1.24^{+0.03}_{-0.04}$
	n_g ^d	$-13.00^{+3.75}_{-4.03}$	$-23.55^{+6.61}_{-6.62}$	> -9.30	$-35.8^{+20.8}_{-30.0}$
Total	EW (eV)	-44^{+17}_{-17}	-59^{+16}_{-16}	-23^{+23}_{-32}	-81^{+47}_{-68}
	f_{obs} (0.3-8 keV) ^e	12.44	16.93	6.52	40.25
	f_{int} (0.3-8 keV) ^e	15.18	20.88	7.76	46.58
χ^2_g	L_{int} (0.3-8 keV) ^f	0.68	0.95	0.35	2.11
	χ^2/dof	134/156	101/119	85/88	29/38
	χ^2_1/dof	144/158	107/121	---	---
	χ^2_{12}/dof	170/160	140/123	85/88	33/40
	χ^2_{123}/dof	189/162	162/125	85/88	39/42
					31/63
					32/65
					34/67

^aParameter values for EPIC PN, ASCA-SIS and CHANDRA-ACIS data.

^bBlackbody normalization in units of $10^{-5} \times 10^{39} \text{ erg s}^{-1}/(d/10 \text{ kpc})^2$, where d is the distance.

^cPower-law normalization in units of $10^{-5} \text{ photons cm}^{-2} \text{ s}^{-1} \text{ keV}^{-1}$ at 1 keV.

^dGaussian normalization in unit of $10^{-6} \text{ photons cm}^{-2} \text{ s}^{-1}$

^eFlux in the unit of $10^{-13} \text{ erg cm}^{-2} \text{ s}^{-1}$

^fSource luminosity in the unit of $10^{44} \text{ erg s}^{-1}$

^g χ^2_1 : excluding Gaussian 1, χ^2_{12} : excluding Gaussian 1 & 2, χ^2_{123} : excluding all Gaussian lines

TABLE 2
ABSORPTION LINES IDENTIFIED IN THE PARAMETRIC FIT TO THE SPECTRUM OF PG 1404+226.

E_{source} (keV)	EW (eV)	$\Delta\chi^2/dof$	Instrument	E_{lab} (keV)	Line	velocity (km s ⁻¹)
$1.00^{+0.01}_{-0.02}$	-46^{+17}_{-9}	18/119	EPIC-PN	0.921	Ne IX 1s-2p	25700^{+3300}_{-6500}
$1.17^{+0.02}_{-0.02}$	-61^{+26}_{-16}	17/117	EPIC-PN	1.022	Ne X Ly α	43500^{+5900}_{-5900}
				1.073	Ne IX 1s-3p	27000^{+5700}_{-5500}
$1.24^{+0.03}_{-0.04}$	-81^{+47}_{-68}	6/40	ASCA-SIS0	1.022	Ne X Ly α	64000^{+8800}_{-11800}
				1.211	Ne X Ly β	7200^{+7400}_{-7200}
$1.59^{+0.10}_{-0.08}$	-87^{+87}_{-68}	5/38	ASCA-SIS0	1.47	Mg XII L α	24500^{+20000}_{-16000}
				1.211	Ne X Ly β	94000^{+20500}_{-16300}
$3.07^{+0.06}_{-0.16}$	-364^{+208}_{-165}	10/154	EPIC-PN	2.62	S XVI Ly α	51500^{+6900}_{-18300}

We use the data obtained from the High Energy Astrophysics Science Research Archive Center (HEASARC), provided by National Aeronautics and Space Adminis-

tration (NASA). SD acknowledges KR scholarship of the TIFR Endowment Fund.

REFERENCES

- Boller, T., Brandt, W. N., & Fink, H. 1996, A&A, 305, 53
 Boroson, T. A., & Green R. F. 1992, ApJS, 80, 109
 Comastri A., Molendi S., & Ulrich M.-H. 1997, In: Makino F., Mitsuda K. (eds.) X-ray imaging and Spectroscopy of Cosmic Hot Plasma. 279
 Dasgupta, S., Rao, A. R., Dewangan, G. C. 2004, ApJ, 614, 626
 Elvis, M., Wilkes, B. J., Lockman, F. J 1989, AJ, 97, 777
 King, A. R. & Pounds, K. A. 2003, MNRAS, 345, 657
 Leighly, K. M., Mushotzky, R. F., Nandra, K., & Forster, K. 1997, ApJ, 489, L25
 Leighly, K. M. 1999, ApJS, 125, 317
 Pounds, K. A., Reeves, J. N., King, A. R., Page, K. L., O'Brien, P. T. & Turner, M. J. L 2003, MNRAS, 345, 705
 Pounds, K. A., King, A. R., Page, & K. L., O'Brien 2003, MNRAS, 346, 1025
 Ulrich, M.-H., Comastri A., Komossa S., & Crane P. 1999, A&A, 350, 816
 Ulrich, M.-H., & Molendi S. 1996, ApJ, 457, 77